Inorg. Chem. **2003**, *42*, 5513–5522

Intermetallic Interactions in Face-to-Face Homo- and Heterodinuclear Bismacrocyclic Complexes of Copper(II) and Nickel(II)

Agnieszka Więckowska,[†] Renata Bilewicz,*[,†] Sławomir Domagała,[†] Krzysztof Woźniak,*[,†] Bohdan Korybut-Daszkiewicz,*[,‡] Alina Tomkiewicz,[§] and Jerzy Mroziński[§]

Chemistry Department, Warsaw University, 02-093 Warszawa, Pasteura 1, Poland, Institute of Organic Chemistry, Polish Academy of Sciences, 01-224 Warszawa, Kasprzaka 44/52, Poland, and Chemistry Department, University of Wroclaw, 50-383 Wroclaw, F. Joliot-Curie 14, Poland

Received February 5, 2003

New face-to-face heterodinuclear complexes containing copper(II) and nickel(II) in identical tetraazamacrocyclic environments have been synthesized and characterized using ESI mass-spectrometry, X-ray diffraction, spectroscopic methods, and elemental analysis. These new bismacrocyclic systems were compared with the respective mono- and bismacrocyclic and [2]catenane homonuclear complexes. Interactions between the metal centers were monitored by magnetic and electrochemical measurements. Magnetic data indicate that all copper compounds studied behave as weakly interacting magnets. In the case of copper [2]catenane, the extent of magnetic interactions decreased when a benzocrown moiety was introduced between the macrocyclic units. On the basis of electrochemical data, the interactions between the metal centers were found to be substantially larger for the nickel complexes than for the corresponding copper ones. Interlocking of a benzocrown ether to form [2]catenane led to a nonequivalence of the metal centers and to the increase of donor abilities of the catenane compared to the respective bismacrocyclic complex. This is reflected by the shift of the first formal potential to less positive values. Intermetallic interactions for the heteronuclear nickel/copper complexes were found intermediary compared to the homonuclear ones. They were strengthened by shortening the spacer between the two tetraazamacrocyclic subunits which is a convenient way of fine-tuning the interactions. The increase of intermetallic interactions led to the increased stability of the intermediate mixed-valence states indicated by the higher values of comproportionation constants.

Introduction

Tailored synthesis of homonuclear bismacrocyclic complexes of transition metal ions can be used to control the strength of interactions between two identical metal centers.[1−3] A strong intramolecular interaction was also found in novel catenated structures prepared using the templating principle and the donor−acceptor attraction between the interlocked units: a bismacrocyclic complex, a benzocrown ether.[4]

Linear scan and differential pulse voltammetries were used to follow the changes of formal potentials of the redox centers induced by the inter- and intramolecular interactions in the compounds studied. Kaifer and co-workers[5] demonstrated that the electroactive centers of [2]catenanes based on bis(paraquat) cyclophane are reduced at more negative potentials when interlocked with benzocrown molecules, due to interactions with the electron rich hydroquinol unit. Also the hydroquinol oxidation is displaced to more positive potentials reflecting the interaction with the π-electron-acceptor paraquat component. The redox behavior of molecules with multiple identical redox sites has been considered by several authors.[6−9] In the case of noninteracting centers, the difference in the formal potentials of the two steps is

* To whom correspondence should be addressed. E-mail: kwozniak@chem.uw.edu.pl (K.W.). Tel./Fax: +48 22 8222892 (K.W.).
† Warsaw University.
‡ Polish Academy of Sciences.
§ University of Wroclaw.

(1) Kaifer, A. E.; Gomez-Kaifer, M. *Supramolecular Chemistry*; Wiley-VCH: Weinheim, Germany, 1999. Myers, R. L.; Shain, I. *Anal. Chem.* **1969**, *41*, 980−990. Polcyn, D. S.; Shain, I. *Anal. Chem.* **1966**, *38*, 370−375.
(2) Bilewicz, R.; Więckowska, A.; Korybut-Daszkiewicz, B.; Olszewska, A.; Woźniak, K.; Feeder, N. *J. Phys. Chem. B* **2000**, *104*, 11430−11434.
(3) Grochala, W.; Jagielska, A.; Woźniak, K.; Więckowska, A.; Bilewicz, R.; Korybut-Daszkiewicz, B.; Bukowska, J.; Piela, L. *J. Phys. Organ. Chem.* **2001**, *14*, 63−73.
(4) Korybut-Daszkiewicz, B.; Więckowska, A.; Bilewicz, R.; Domagała, S.; Woźniak, K. *J. Am. Chem. Soc.* **2001**, *123*, 9356−9366.
(5) Lu, T.; Zhang, L.; Gokel, G. W.; Kaifer, A. E. *J. Am. Chem. Soc.* **1993**, *115*, 2542−2543.

10.1021/ic034127b CCC: $25.00
Published on Web 08/05/2003

determined by simple statistics. The magnitude of separation between the formal potentials of each site is a measure of the extent of interaction between the two redox sites. When the interactions are weaker, the difference between the two formal potentials, ΔE_o, decreases. For a small delocalization energy in homodinuclear systems, the redox potential separation includes two contributions: the intersite electron−electron repulsion; the coupling of metal centers.[8] Resonance stabilization due to the coupling of the metal centers may not be a major factor in determining the comproportionation constant and—as shown in many weakly coupled mixed-valence complexes—the electrostatic repulsion between metal centers will favor the mixed-valence state relative to the isovalent forms.[8,9]

In the case of two nonidentical redox sites, the electronic effect of one redox center may affect the behavior of the second one. In this paper, therefore, we present three novel bismacrocyclic structures with nonidentical metal centers and compare them with the respective homonuclear complexes. We also describe factors which determine the extent of interaction of the neighboring metal sites: the length of the spacer controlling intersite separation; the type of metal ion occupying given centers; the presence of interlocked molecules. These factors are reflected in the values of formal potentials related to the structure of the bismacrocyclic complexes.

Experimental Section

Voltammetry. Voltammetric experiments were accomplished using the Autolab potentiostat (ECO Chemie, The Netherlands) in a three-electrode arrangement with a silver−silver chloride electrode as the reference, platinum foil as the counter, and glassy carbon electrode (GCE, BAS, 3 mm diameter) as the working electrode. The reference electrode was a Ag/AgCl electrode separated from the working solution by an electrolytic bridge filled with 0.1 M TBAHFP/AN (tetrabutylammonium hexafluorophosphate/acetonitrile) solution. The reference electrode potential was calibrated by using the ferrocene oxidation process in the same 1 M TBAHFP/AN solution. Acetonitrile (AN) containing 0.1 M TBAHFP was used as the supporting electrolyte solution. Argon was used to deaerate the solution, and an argon blanket was maintained over the solution during the experiments. Formal potentials were obtained through a fitting procedure using the COOL program for the single couple of peaks corresponding to the Me^{II}/Me^{III} system and assuming E_1E_2 is a reversible process.[10]

Magnetic Measurements. Magnetic measurements were accomplished using a Quantum Design SQUID magnetometer (type MPMS-XL-5) in the temperature range from 1.9K up to 300K. The SQUID magnetometer was calibrated with a palladium rod sample (Materials Research Corp., measured purity 99.9985%) for which the gram magnetic susceptibility was taken as 5.30×10^{-6} cm^3 g^{-1} at 293 K (National Bureau of Standards, Bethesda, MD).[11] All susceptibility measurements were made in a field of 5 kG. The corrections for diamagnetism of the constituent atoms were calculated from the Pascal constants.[12]

Spectroscopic Measurements. IR spectra (paraffin oil mulls) were recorded with a Perkin-Elmer Spectrum 2000 Ft-IR spectrometer, and electronic spectra, on a Cary 1E UV−visible spectrometer. ESI mass spectra were measured on a Mariner Perseptive Biosystem mass spectrometer. Solid-state electron paramagnetic resonance (EPR) spectra were recorded on a Bruker ER 200 E-SRC spectrometer at temperatures of 77 and 300 K and for a magnetic field range of 0−10 kG.

Synthesis. The solvents and reagents used in these studies was reagent grade or better. Acetonitrile was dried over P_2O_5 and distilled under argon. Homodinuclear complexes **3−7CuCu, 9CuCu**, **3−7NiNi**, and **9NiNi**[4] as well as the dihexafluorophosphate salts **1Cu, 8Cu, 1Ni**, and **8Ni** were synthesized according to the previously published procedures.[3,4]

[6,13-Bis(((7′-ammonioheptyl)amino)methylidene)-1,4,8,11-tetrazacyclotetradeca-4,7,11,14-tetraene-$\kappa^4N^{1,4,8,11}$]copper(II) Tetrahexafluorophosphate (2Cu-7). A solution of complex **1Cu** (0.635 g, 1 mmol) in 50 mL of dry acetonitrile was added during 2 h to a vigorously stirred solution of heptanediamine (1.3 g, 10 mmol) in 50 mL of the same solvent. The mixture was stirred for 1 h at room temperature, acidified with concentrated hydrochloric acid (2 mL), and diluted with water (200 mL). The resulting solution was applied on 2 × 20 cm SP Sephadex C-25 column. The column was washed with water and eluted with 0.5 M Na_2SO_4 solution. The major red band was collected and the product precipitated upon addition of an excess of ammonium hexafluorophosphate. The precipitate was filtered off, dissolved in acetonitrile containing a small amount of ammonium hexafluorophosphate, and diluted with water. The red product precipitating upon evaporation of acetonitrile was filtered off and dried under reduced pressure. Yield: 0.730 g, 65%. The second red band was eluted with 0.5 M NaCl solution and precipitated upon addition of ammonium hexafluorophosphate. The second band was proved by ESI MS to contain mainly 2:3 condensation product (*m*/*z*: 188.7, $[C_{45}H_{80}N_{14}Cu_2 - 1H^+]^{5+}$; 235.6, $[C_{45}H_{80}N_{14}Cu_2 - 2H^+]^{4+}$l 761.1, $[C_{45}H_{80}N_{14}Cu_2(PF_6)_4]^{2+}$). Anal. Calcd for $C_{26}H_{50}N_8Cu(PF_6)_4$ (M_r = 1118.14): C, 27.9; H, 4.5; N, 10.0. Found: C, 27.7; H, 4.6; N, 10.0. ESI MS (*m*/*z*): 178.8, $[C_{26}H_{50}N_8Cu - 1H^+]^{3+}$; 227.5, $[C_{26}H_{50}N_8Cu(PF_6)]^{3+}$.

[6,13-Bis(((5′-ammoniopentyl)amino)methylidene)-1,4,8,11-tetrazacyclotetradeca-4,7,11,14-tetraene-$\kappa^4N^{1,4,8,11}$]copper(II) tetrahexafluorophosphate (2Cu-5) and [6,13-Bis(((3′-ammoniopropyl)amino)methylidene)-1,4,8,11-tetrazacyclotetradeca-4,7,11,14-tetraene-$\kappa^4N^{1,4,8,11}$]copper(II) tetrahexafluorophosphate (2Cu-3) were obtained by following the same procedure as above. Data for **2Cu-5** are as follows. Yield: 61%. Anal. Calcd for $C_{22}H_{42}N_8Cu(PF_6)_4 \cdot 4H_2O$ (M_r = 1134.09): C, 23.3; H, 4.4; N, 9.9. Found: C, 23.1; H, 4.3; N, 10.0. ESI MS (*m*/*z*): 160.1, $[C_{22}H_{42}N_8Cu - 1H^+]^{3+}$; 239.6, $[C_{26}H_{50}N_8Cu - 2H^+]^{2+}$. Complex **2Cu-3** decomposed during crystallization to form bismacrocycle **3CuCu**[4] and therefore has not been characterized analytically. Also the peaks characteristic of **3CuCu** were observed as a major component in the ESI mass spectra. Complex **2Cu-3** used in the synthesis of **3CuNi** contained ca. 10% **3CuCu**. Yield: ca. 40%.

[3,11,15,18,22,30,34,37,41,44,46,49-Dodecaazatricyclo[26.6.6.6^{13,20}]pentaconta-1,12,14,18,20,31,33,37,39,43,45,49-

(6) Flanagan, J. B.; Margel, S.; Bard, A. J.; Anson, F. C. *J. Am. Chem. Soc.* **1978**, *100*, 4248−4253.
(7) Ammar, F.; Savéant, J.-M. *Electroanal. Chem.* **1973**, *47*, 215−221.
(8) Richardson, D. E.; Taube, H. *Coord. Chem. Rev.* **1984**, *60*, 107−129.
(9) Girerd, J. J.; Anxolabbehere-Mallart, E. In *Spectroscopic Methods in Bioinorganic Chemistry*; Solomon, E. I., Hodgson, K., Eds.; American Chemical Society: Washington, DC, 1997; pp 262−271.
(10) *Model 271 COOL, Kinetic Analysis Software*; EG&G Instruments Corp.: 1992.
(11) Briscoe, H. V. A.; Robinson, P. L.; Rudge, A. J. *J. Chem. Soc.* **1931**, 3219.
(12) König, E. *Magnetic Properties of Coordination and Organometallic Transition Metal Compounds*; Springer-Verlag: Berlin, 1966.

dodecaene-1$\kappa^4N^{34,37,41,44}$,2$\kappa^4N^{15,18,46,49}$]copper(II)nickel(II) Tetrahexafluorophosphate (7CuNi). A solution of diisopropylethylamine (0.120 g, 0.5 mmol) in 20 mL of acetonitrile was slowly added (1 h) to the mixture of **2Cu-7** (0.230 g, 0.25 mmol) and **1Ni** (0.156 g, 0.25 mmol) complexes dissolved in 100 mL of dry acetonitrile. The mixture was stirred at room temperature for the next 3 h. Then, the solvent was removed by rotary evaporation to give a dark brown residue. The residue was dissolved in a small volume of acetonitrile and absorbed on the neutral alumina column (2 × 25 cm). The column was eluted with acetonitrile solution of NH_4PF_6 (1 g/100 mL). The red fast moving band was collected, concentrated, and diluted with water. Red product (**7CuNi**), precipitated upon evaporation of acetonitrile, was filtered off, washed with water, and dried in vacuo. Yield: 0.170 g (49%). Anal. Calcd for $C_{38}H_{60}N_{12}CuNi(PF_6)_4$ (M_r = 1387.07): C, 32.9; H, 4.4; N, 12.1. Found: C, 32.9; H, 4.5; N, 11.9. IR (Nujol, cm^{-1}): 3390, 1658, 1633 vs, 1569, 835 vs, 557. UV/vis (acetonitrile) [λ_{max} (ϵ_{max})]: 347 (85 300), 469 sh (1250). ESI MS (*m*/*z*): 201.8, [$C_{38}H_{60}N_{12}CuNi]^{4+}$; 317.4, [$C_{38}H_{60}N_{12}CuNi\cdot(PF_6)]^{3+}$; 548.6, [$C_{38}H_{60}N_{12}CuNi(PF_6)_2]^{2+}$.

[3,7,11,14,18,22,26,29,32,35,38,41-Dodecaazatricyclo[22.6.6.6^{9,16}]dotetraconta-1,8,10,14,16,23,25,29,31,35,37,41-dodecaene-1$\kappa^4N^{26,29,31,35}$-2$\kappa^4N^{11,14,37,41}$]copper(II)nickel(II) Tetrahexafluorophosphate (3CuNi). The complex **2Cu-3** (0.27 g, 0.25 mmol) was dissolved in dry acetonitrile and evaporated to dryness to remove water of crystallization. The residue was dissolved in 100 mL of dry acetonitrile containing **1Ni** (0.16 g, 0.25 mmol), and diisopropylethylamine (0.12 g, 0.5 mmol) solution in 20 mL of acetonitrile was slowly added (1 h) to the mixture. The mixture was stirred for 3 h at room temperature, after which (2 mL) concentrated hydrochloric acid was added. The brown precipitate was filtered off and dissolved in water (50 mL), and the resulting solution was absorbed on a 2 × 20 cm SP Sephadex C-25 column. The column was washed with water and eluted with 0.5 M Na_2SO_4 solution. The first 3 bands were collected (red, red, yellow) were collected and the products precipitated upon addition of ammonium hexafluorophosphate. The precipitates were filtered off, dissolved in acetonitrile containing a small amount of ammonium hexafluorophosphate, and diluted with ethanol. Products precipitated upon slow evaporation of acetonitrile were filtered off, washed with ethanol, and dried under reduced pressure. First and third fractions contained **3CuCu** (0.05 g, 15%) and **3NiNi** (0.03 g, 10%) impurities, respectively (ESI MS). Yield: 0.05 g, 15%. Anal. Calcd for $C_{30}H_{44}N_{12}CuNi(PF_6)_4\cdot H_2O$ (M_r = 1292.87): C, 27.9; H, 3.6; N, 13.0. Found: C, 28.0; H, 3.7; N, 13.1. IR (Nujol, cm^{-1}): 3372, 1661, 1625 vs, 1587, 846 vs, 559. UV/vis (acetonitrile) [λ_{max} (ϵ_{max})]: 345 (31 200), 468 sh (1290). ESI MS (*m*/*z*): 173.3, [$C_{30}H_{44}N_{12}CuNi]^{4+}$; 231.4, [$C_{30}H_{44}N_{12}CuNi - 1H^+]^{3+}$; 279.4, [$C_{30}H_{44}N_{12}CuNi(PF_6)]^{3+}$; 418.6, [$C_{30}H_{44}N_{12}CuNi(PF_6) - 1H^+]^{2+}$.

[3,9,13,16,20,26,30,33,37,40,42,45-Dodecaazatricyclo[26.6.6.6^{11,18}]hexatetraconta-1,10,12,16,18,27,29,33,35,39,41,45-dodecaene-1$\kappa^4N^{30,33,36,39}$-$\kappa^4N^{13,16,42,45}$]copper(II)nickel(II) hexafluorophosphate *(5CuNi)* was obtained by following the same procedure as above. The impurity of **5CuCu** was separated as a first band, and **5NiNi** remained permanently absorbed on the SP Sephadex C-25 column. Yield: 40%. Anal. Calcd for $C_{34}H_{52}N_{12}CuNi(PF_6)_4\cdot 3H_2O$ (M_r = 1385.01): C, 29.5; H, 4.2; N, 12.1. Found: C, 29.5; H, 4.2; N, 12.1. IR (Nujol, cm^{-1}): 3392, 1664, 1625 vs, 1572, 840 vs, 557. UV/vis (acetonitrile) [λ_{max} (ϵ_{max})]: 345 (72 000), 465 sh (1380). ESI MS (*m*/*z*): 187.8, [$C_{34}H_{52}N_{12}CuNi]^{4+}$; 298.0, [$C_{34}H_{52}N_{12}CuNi(PF_6)]^{3+}$; 519.5, [$C_{34}H_{52}N_{12}CuNi(PF_6)_2]^{2+}$.

X-ray Determinations. All single-crystal X-ray measurements of **3CuCu** and **3CuNi** were performed on a Kuma KM4CCD κ-axis diffractometer with graphite-monochromated Mo Kα radiation at 100 K. The crystal was positioned at 65 mm from the KM4CCD camera. For **3CuCu** 856 frames were measured at 1.4° intervals with a counting time of 40 s, whereas for **3CuNi** 924 frames were measured at 1.3° intervals with a counting time of 40 s. The data were corrected for Lorentz and polarization effects. No absorption correction was applied. Data reduction and analysis were carried out with the Kuma Diffraction (Wrocław) programs.

The structures were solved by direct methods[13] and refined using SHELXL.[14] The refinement was based on F^2 for all reflections except those with very negative F^2. Weighted R factors wR and all goodness-of-fit *S* values are based on F^2. Conventional R factors are based on *F* with *F* set to zero for negative F^2. The $F_o^2 > 2\sigma(F_o^2)$ criterion was used only for calculating R factors and is not relevant to the choice of reflections for the refinement. The R factors based on F^2 are about twice as large as those based on *F*. All hydrogen atoms were located in ideal geometrical positions. Some of the non-hydrogen atoms were refined isotropically because of poor diffraction. Scattering factors were taken from Tables 6.1.1.4 and 4.2.4.2 in ref 15.

Crystallographic data (excluding structure factors) for the structures reported in this paper have been deposited with the Cambridge Crystallographic Data Center and allocated the deposition numbers CCDC 188407 and CCDC 188408 for **3CuCu** and **3CuNi**, respectively. Copies of the data can be obtained free of charge on application to CCDC, 12 Union Road, Cambridge CB2 1EW, U.K. (fax, int code + (1223)336-033; E-mail, deposit@ccdc.cam.ac.uk).

3CuCu: $Cu_2C_{30}N_{12}H_{48}P_4F_{24}O_2$, fw = 1315.73; T = 100 K; λ = 0.710 73 Å; orthorhombic; space group, $P2_12_12_1$; unit cell dimensions, a = 14.216(3) Å, b = 18.233(4) Å, c = 18.363(4) Å, V = 4759.7(16) Å^3; Z = 4; density (calcd) = 1.837 Mg/m^3; absorption coefficient = 1.17 mm^{-1}; F(000) = 2648; crystal size = 0.10 × 0.08 × 0.05; θ range for data collection = 3.08−21°; index ranges: $-14 \le h \le 14$, $-18 \le k \le 18$, $-18 \le l \le 18$; reflections collected = 25 598; independent reflections = 5102 [R_{int} = 0.303]; refinement method, full matrix least squares on F^2; data/restraints/parameters = 5102/0/298; goodness-of-fit on F^2 = 0.869; final R indices [$I > 2\sigma(I)$], R1 = 0.1052 and wR2 = 0.1584; R indices (all data), R1 = 0.2224, wR2 = 0.2312, extinction coefficient = 0; weight = $1/[\sigma^2(F_o^2) + (0.0000P)^2 + 0.00P]$, where $P = (\max(F_o^2, 0) + 2F_c^2)/3$; largest diffraction peak and hole = 0.55 and −1.14 e Å^{-3}.

3CuNi: $NiCuC_{30}N_{12}H_{48}P_4F_{24}O_2$, fw = 1310.90; T = 100 K; λ = 0.710 73 Å; orthorhombic; space group, $P2_12_12_1$; unit cell dimensions, a = 14.218(3) Å, b = 18.236(4) Å, c = 18.380(4) Å, V = 4765.6(16) Å^3; Z = 4; density (calcd) = 1.82 Mg/m^3; absorption coefficient = 1.12 mm^{-1}; F(000) = 2628; crystal size = 0.10 × 0.08 × 0.05; θ range for data collection = 3.08−21°; index ranges $-14 \le h \le 14$, $-18 \le k \le 18$, $-18 \le l \le 18$; reflections collected = 25 434; independent reflections = 5108 [R_{int} = 0.242]; refinement method, full matrix least squares on F^2; data/restrains/parameters = 5108/0/298; goodness-of-fit on F^2 = 0.900; final R indices [$I > 2\sigma(I)$], R1 = 0.0858 and wR2 = 0.1476; R indices (all data), R1 = 0.1851, wR2 = 0.2035, extinction coefficient = 0; weight = $1/[\sigma^2(F_o^2) + (0.0358P)^2 + 0.00P]$, where $P = (\max(F_o^2, 0) + 2F_c^2)/3$; largest diffraction peak and hole = 0.68 and −0.58 e Å^{-3}.

(13) Sheldrick, G. M. *Acta Crystallogr*. **1990**, *A46*, 467−473.
(14) Sheldrick, G. M. *SHELXL93. Program for the Refinement of Crystal Structures*; University of Göttingen: Göttingen, Germany.
(15) *International Tables for Crystallography*; Wilson, A. J. C., Ed.; Kluwer: Dordrecht, Germany, 1992; Vol. C.

Scheme 1

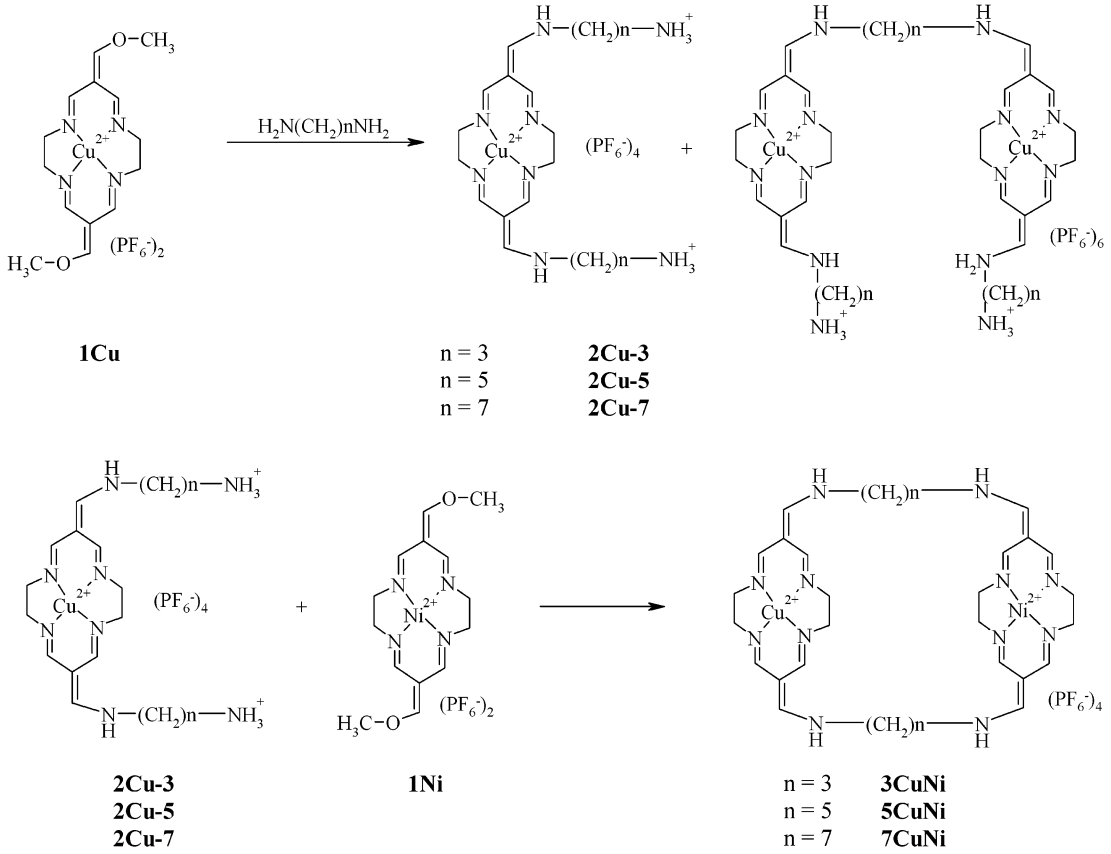

Results and Discussion

The synthesis of heterodinuclear complexes **3**−**7CuNi** is summarized in Scheme 1. The reaction of enol ether **1Cu** with an excess of appropriate diamine gave the mixture of protonated bis(diamino)-substituted [14]cyclidene complexes **2Cu** as well as 2:3 condensation products, which were then separated by chromatography on an SP Sephadex C-25 column. Further condensation of **2Cu** with **1Ni** in the presence of base gave face-to-face bismacrocyclic complexes **3**−**7CuNi**. An opposite sequence of reactions leads to the same products; however, the isolation and purification of **2Ni** bis(diamino) derivatives were more difficult.

Structural Details of Compounds 3CuNi and 3CuCu. In general, the structures of **3CuNi** and **3CuCu** (Figure 1) are similar to that previously described for bismacrocycle **3NiNi**.[4] All compounds differ by one metal atom in the formula. Because of the lack of the inversion center, both compounds crystallize in the orthorhombic $P2_12_12_1$ space group with very similar unit cell dimensions.

Each molecule is comprised of two macrocycles which close the cycle cavity, linked by aliphatic chains. The dimensions of such a cavity (Table 1) for **3CuNi** are equal to 4.37 Å (Ni···Cu) × 14.68 Å (C11A···C11B) and for **3CuCu** 4.36 Å (Cu···Cu) × 14.61 Å (C11A···C11B), which is very similar to 4.46 Å (Ni···Ni) × 14.61 Å (for C11A···C11B) in **3NiNi**. The shorter length of the Ni···Cu contact than that for Ni···Ni is explained by the different strength of the interactions between the metallic centers. All other important interatomic distances are given in Table 1. There is only a slight difference of 1 electron between Ni^{II} and Cu^{II} cations, which is difficult to differentiate by X-ray diffraction. However, the assignment of ions can be done by the use of average Me···N distances, which are different for both cations.

Positively charged bismacrocyclic complex cations **3CuNi** and **3CuCu** are surrounded by negatively charged counterions and water molecules (Figure 2). They surround bismacrocycles in a symmetric way creating a pseudosymmetric environment and forming a number of hydrogen bonds (see Supporting Information Table S1). Both the bismacrocyclic cations interact strongly with some water molecules. However, because of poor diffraction even at low temperature (100 K), we were unable to locate the water hydrogen atoms directly from difference Fourier maps.

There are four CH−NH−CH_2 groups in both bismacrocycles—two for each macrocyclic unit. The two CH−NH−CH_2 groups, linked with the same macrocycle, are located cis relative to each other whereas when the same CH−NH−CH_2 groups are linked by the aliphatic linkers −$(CH_2)_3$−, their relative location is trans (see Figure 2). In general, there can be cis or trans isomerism both on the macrocyclic units as well as on the ends of the aliphatic linkers.

Electrochemistry. Comparison of Redox Properties of Binuclear and Mononuclear Complexes. Monomacrocyclic complexes **8Cu** and **8Ni** (Chart 1) exhibit close to reversible Me^{II}/Me^{III} electrode processes (Figures 3 and 4). In homo-

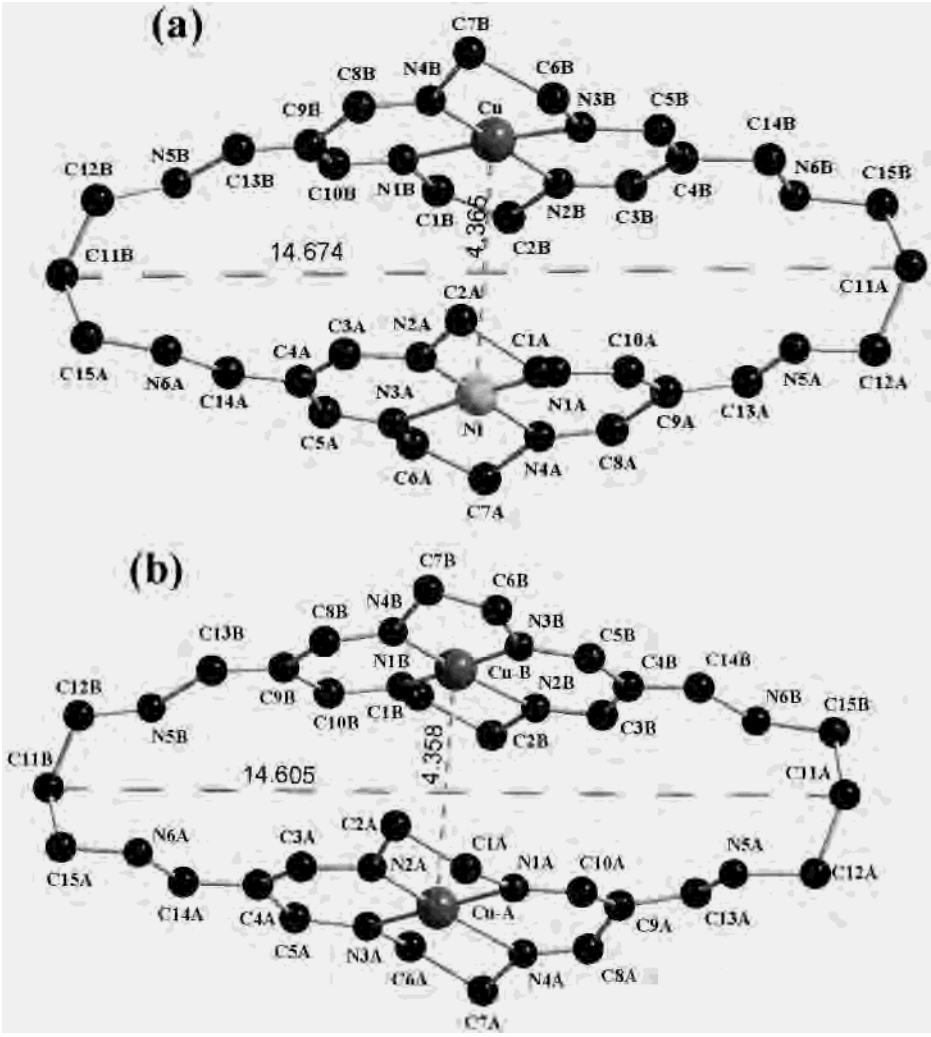

Figure 1. Atomic labels and the definition of the molecular void created by (a) **3CuNi** and (b) **3CuCu.** Counterions, water molecules, and hydrogen atoms are omitted for the sake of clarity.

Table 1. Most Important Interatomic Distances (Å) for Dinuclear Complexes **3MeMe**

	bismacrocyclic complex		
param definition	**3CuCu**	**3CuNi**	**3NiNi**[4]
M−A···M−B	4.358(5)	4.365(3)	4.464(2)
C11A···C11B	14.61(4)	14.67(2)	14.61(2)
C4A···C9B	3.99(5)	4.06(4)	4.11(1)
C4B···C9A	4.01(4)	4.01(4)	4.11(1)
N5A···N6B	3.07(3)	2.84(3)	3.03(1)
N5B···N6A	2.89(4)	3.16(3)	3.03(1)
M−A···N1A	1.97(2)	1.76(2)	1.843(6)
M−A···N2A	1.80(2)	1.83(2)	1.845(6)
M−A···N3A	1.94(2)	1.91(2)	1.855(6)
M−A···N4A	2.09(3)	1.87(2)	1.859(6)
M−B···N1B	1.72(3)	2.02(2)	1.843(6)
M−B···N2B	2.03(3)	1.93(2)	1.845(6)
M−B···N3B	1.74(3)	1.87(2)	1.855(6)
M−B···N4B	1.78(2)	1.93(2)	1.859(6)

nuclear bismacrocyclic complexes the redox potentials for the copper centers are shifted to more positive values compared to that of the corresponding monomacrocyclic compound (Table 2).

When the spacer length in the Cu^{II} and Ni^{II} in bismacrocyclic complexes is decreased from $n = 7$ to $n = 3$ (Table 2), the formal potentials are displaced to more positive values. This can be interpreted in terms of increasing electrostatic repulsion between the centers. For the longest spacer the formal potential is approaching the value for the respective mononuclear complex.

For bismacrocyclic Ni^{II} complexes the shape of the voltammetric curve depends also on the length of the spacer. In the case of **3NiNi**, the splitting of the peaks into two indicates some stabilization of the intermediate mixed-valence state compared to the copper analogue where no splitting is observed. The stability of the mixed-valence complex is exhibited by the extent of splitting of the formal potentials which can be observed by electrochemistry or by the appearance of an intervalence-transfer absorption band as previously observed in the near-infrared region with some other intervalent compounds.[6,17] For similar comproportionation constants in cofacial copper porphyrins, lack of these characteristic bands was reported by El-Kasmi et al.[17] and explained by weakness of the interactions.

The splitting is higher for Ni^{II} complexes than for the corresponding Cu^{II} systems, so that two separated couples

(16) Hush, N. S. In *Progress in Inorganic Chemistry*; Cotton, F. A., Ed.; InterScience Publishers: New York, 1967; Vol. 8, pp 357−444.
(17) El-Kasmi, A.; Lexa, D.; Maillard, P.; Momenteau, M.; Savéant, J.-M. *J. Phys. Chem*. **1993**, *97*, 6090−6095.

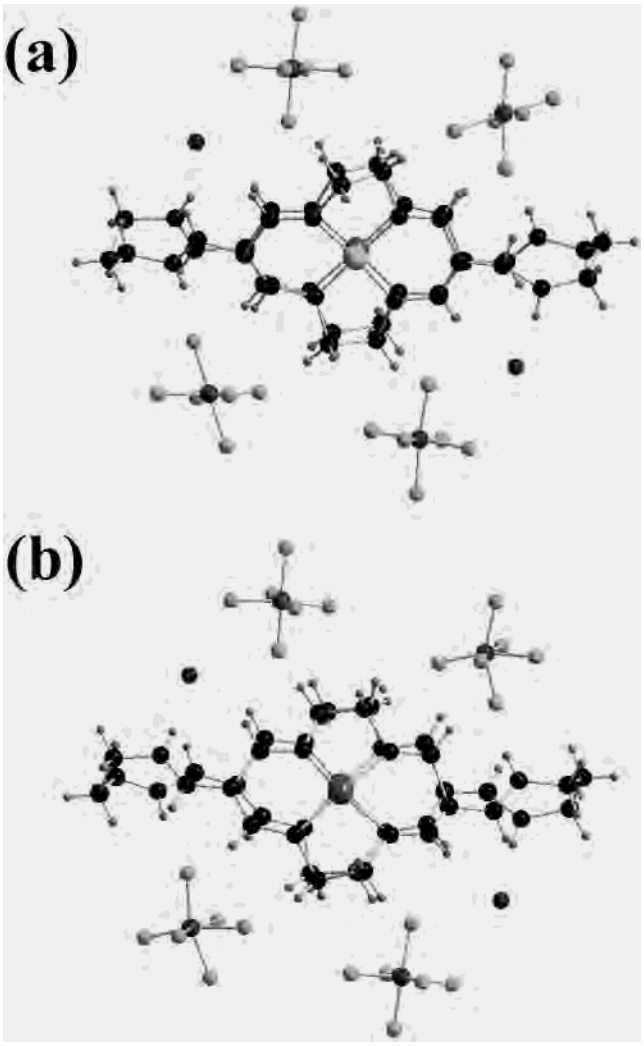

Figure 2. Closest environment of bismacrocyclic complexes consisting of hexafluorophosphate ions and water molecules: (a) **3CuNi**; (b) **3CuCu**.

of peaks can be observed. Interestingly, the intermetallic distances observed in the solid state are also larger for **3NiNi** (4.46 Å for Ni···Ni in **3NiNi**; 4.36 Å for Cu···Cu in **3CuCu**).

For the copper complexes, when the length of the spacer is decreased from 7 to 3 (Table 2), no other changes are seen except further positive shift of the Cu^{II}/Cu^{III} formal potential, which again is in accord with the increasing electrostatic repulsion.

The redox characteristics of the macrocyclic complexes are presented in Table 2. The electrooxidation process for the Ni^{II} complex corresponds to the following scheme:

$$\mathbf{Ni^{II}Ni^{II}} - e \xrightarrow{E_1} \mathbf{Ni^{II}Ni^{III}} - e \xrightarrow{E_2} \mathbf{Ni^{III}Ni^{III}}$$

An additional equilibrium is the disproportionation of $\mathbf{Ni^{II}Ni^{III}}$ complex affecting the shape of the voltammogram:

$$2\mathbf{Ni^{II}Ni^{III}} \leftrightarrow \mathbf{Ni^{II}Ni^{II}} + \mathbf{Ni^{III}Ni^{III}}$$

Here $K_{com} = \exp[(\Delta E_o)F/RT$ and ΔE_o is the standard potential difference between the successive monoelectron transfers. For $K_{com} < 4$, $E_1 - E_2 < 35.6$ mV and the mixed-valence form is unstable.[18,19] When K_{com} is equal to 4, the centers

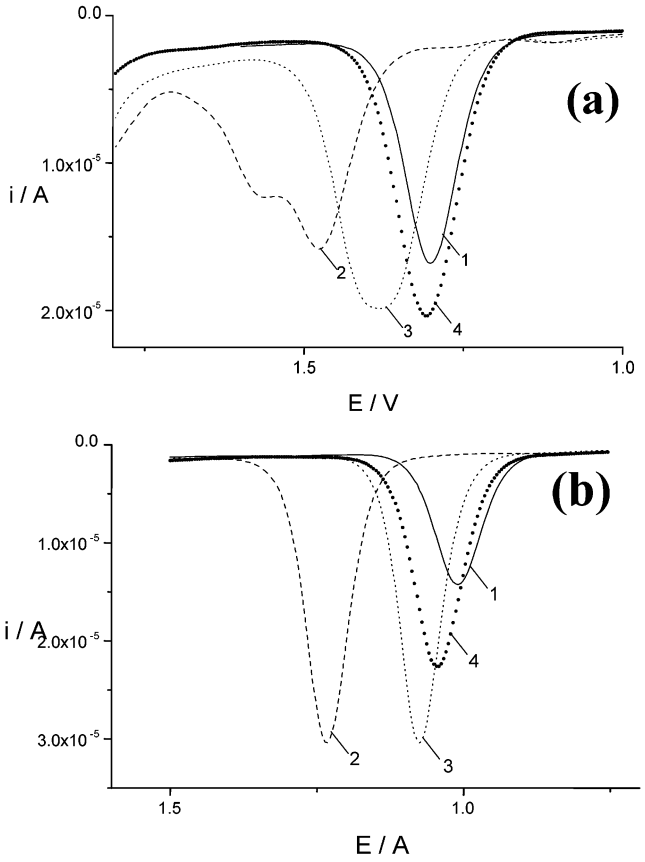

Figure 3. Differential pulse voltammograms for (a) Ni^{II} and (b) Cu^{II} bismacrocyclic complexes recorded using GCE in 1 M TBAHFP AN solution: (a) (1) **8Ni**, (2) **3NiNi**, (3) **5NiNi**, (4) **7NiNi**; (b) (1) **8Cu**, (2) **3CuCu**, (3) **5CuCu**, (4) **7CuCu.** Pulse amplitude: 0.025 V.

Chart 1

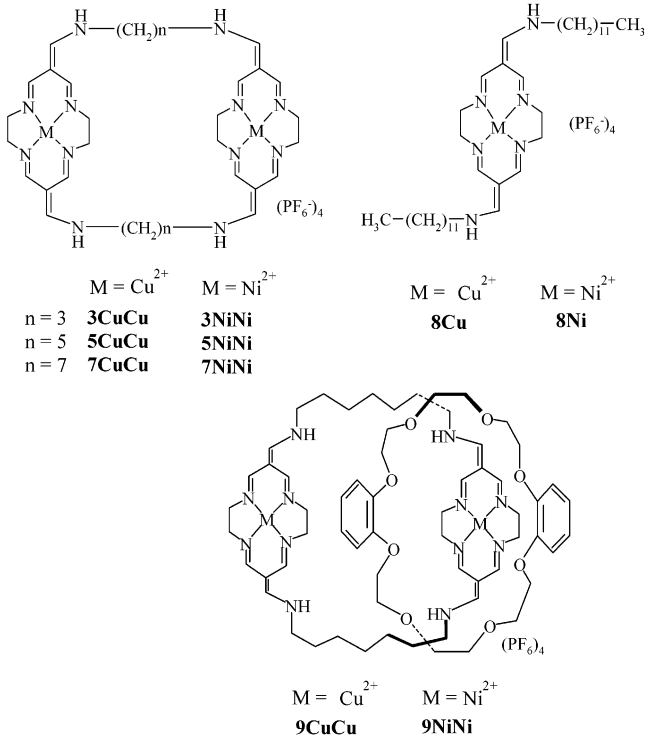

are noninteractive while larger values of K_{com} indicate interaction between the redox centers.

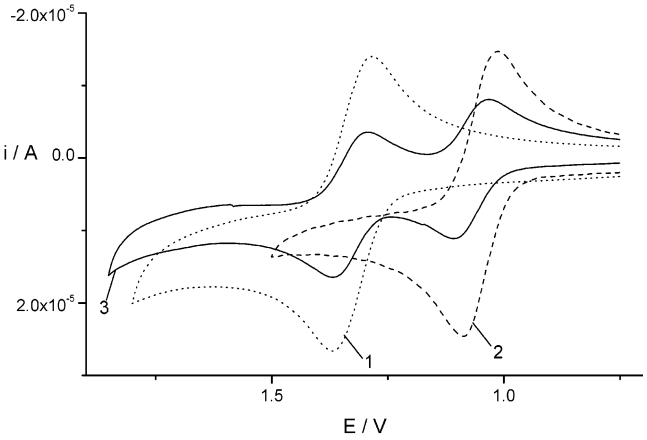

Figure 4. Comparison of cyclic voltammograms for homo- and heterodinuclear complexes of Ni^{II} and Cu^{II} recorded using GCE in 1 M TBAHFP AN solution: (1) **7NiNi** (dotted line); (2) **7CuCu** (dashed line); (3) **7NiCu** (solid line). Scan rate: 0.05 V/s.

Table 2. Comparison of the Redox Properties of Mono- and Bismacrocyclic Complexes of Ni^{II} and Cu^{II}

compd	$E_{pa} - E_{p/2a}$ (V)	$E°_1$ (V)	$E°_2$ (V)	$\Delta E°$ (V)	K_{com}
8Ni	0.063	1.308			
3NiNi		1.485	1.585	0.100	49.5
5NiNi	0.089	1.353[a]	1.432[a]	0.079	21.7
7NiNi	0.072	1.346[a]	1.417[a]	0.071	15.9
9NiNi		1.250	1.391	0.141	243
8Cu	0.058	1.018			
3CuCu	0.055	1.243		0.034	3.80
5CuCu	0.057	1.084		0.037	4.29
7CuCu	0.058	1.052		0.038	4.54
9CuCu	0.075	1.002[a]	1.057[a]	0.055	12.40

[a] Formal potentials obtained by fitting the voltammetric curves to theoretical values using the COOL program.[10]

In the case of Ni^{II} complexes the value of the comproportionation constant increases from 15.9 for **7NiNi** to 49.5 for **3NiNi.** The separation of peaks is clearly seen in the differential pulse voltammetry mode (Figure 3).

Increased Intermetallic Interactions in Catenane Systems. The comparison of **7NiNi** and the catenane electrochemical behavior reveals the strengthening of interactions between the metal centers due to the messenger role of electron-rich component dibenzo-24-crown-8.[4] Linear scan voltammetry peaks of the Ni^{II}/Ni^{III} system are split into two upon interlocking the quinone unit. The value of the comproportionation constant dramatically increases when the interlocking crown unit is incorporated in the bismacrocyclic Ni and Cu complex (Table 2). The comproportionation constant becomes even higher than in the case of the shortest spacer between the tetraazamacrocyclic units. This indicates that catenane structures may be a promising way to stabilize the intervalent compounds in the multicenter redox devices. In the case of the Cu complex (Table 2), interlocking with benzocrown ether induces interactions of the centers, which are otherwise completely independent in the parent bismacrocyclic complex. One can try to rationalize such a significant increase of interactions in the catenanes. Both Ni^{II} and Cu^{II} cations possess d-electrons (d^8 and d^9, respectively). The field exerted by the closest atomic environment (four nitrogen atoms) is—in first approximation—close to a square-planar (D_{4h}) one. Since the nitrogen atoms have their lone electron pairs directed toward the metal centers, the electrons in cationic orbitals pointing toward the nitrogen atoms are repelled more strongly and the corresponding orbitals will be higher in energy. In the case of the catenane complexes the benzocrown unit is electron rich and this will lead to a higher electron population at the metal orbitals close to the benzocrown. In consequence, the onset of oxidation appears at the less positive potentials than in case of respective bismacrocycles or even monomacrocycles.

It should be also stressed that the two centers in catenanes are not equal as it was the case for simple homodinuclear complexes. The microenvironments around each of them are different because of the presence of the interlocked crown ether encircling one of the units; thus, this difference should also contribute to the observed formal potentials separation.

Electrochemistry of Heterodinuclear Systems. The redox properties of homodinuclear complexes of Ni and Cu were compared with those of the corresponding newly prepared heterodinuclear complexes (Figures 4 and 5).

The redox potentials are collected in Table 3. The potentials of the peaks resemble those of the respective homodinuclear complexes for the longest spacer (Figures 4 and 5a). For shorter spacers the interaction of copper and nickel centers leads to a shift of the Ni oxidation peak toward more positive potentials. This peak appears at the potential close to the middle point of the split signal recorded for the respective homodinuclear system (Figure 5c). Following insertion of a different metal center instead of the two identical ones in homodinuclear complexes, the donor abilities are weakened (Table 3)—both formal potentials are shifted to more positive values—thus the overall complex is more difficult to oxidize. On the other hand, the difference of the Cu and Ni formal potentials in mixed complexes is always smaller than the difference of the formal potentials of Cu and Ni centers in homodinuclear complexes. Thus, the interaction between the centers is weakened when two different metals are bound in one molecule (see the Ni center formal potential for **3NiNi** and **3CuNi**; Table 3) and the stability of the mixed complex in its mixed-valence state, $Cu^{III}Ni^{II}$, is increased with the shortening of the linkers binding the two units.

Magnetic Properties. Magnetic susceptibility has been measured in the temperature range 1.90−300K. Figure 6 shows the plots of χ_M vs T and $\chi_M T$ vs T (where χ_M is molar magnetic susceptibility per Cu−Cu unit) for **3CuCu**, **5CuCu**, and **7CuCu** complexes.

In all cases the χ_M value increases slowly with the decrease of temperature, but in the low-temperature region a rapid increase of the molar susceptibility values occurred without showing a maximum. In the $\chi_M T$ vs T plots for **3CuCu** and **5CuCu** complexes, χ_M decreases very slowly in a wide range of temperature. At low temperatures (below 10 K) this value decreases to 0.72 $cm^3\ mol^{-1}$ K for **3CuCu**, 0.73 $cm^3\ mol^{-1}$ K for **5CuCu**, and 0.56 $cm^3\ mol^{-1}$ K for **7CuCu** at 1.90 K.

(18) Gagne, R. R.; Koval, C. A.; Smith, T. J.; Cimolino, M. C. *J. Am. Chem. Soc.* **1979**, *101*, 4571−4580.
(19) Gagne, R. R.; Spiro, C. L.; Smith, T. J.; Hamann, C. A.; Thies, W. R.; Shiemke, A. K. *J. Am. Chem. Soc.* **1981**, *103*, 4073−4081.

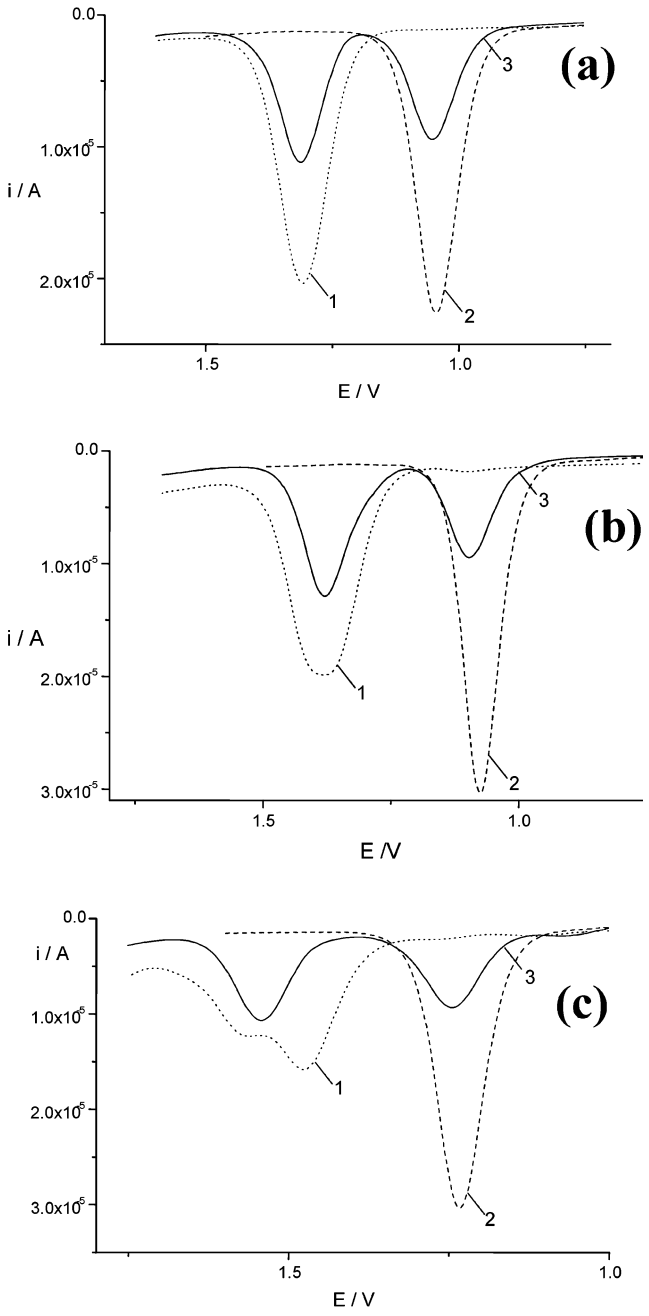

Figure 5. Differential pulse voltammograms for 1 mM (a) Ni^{II} and (b) Cu^{II} dinuclear complexes recorded using GCE in 1 M TBAHFP AN solution: (a) (1) **7NiNi**, (2) **7CuCu**, (3) **7NiCu**; (b) (1) **5NiNi**, (2) **5CuCu**, (3) **5NiCu**; (c) (1) **3NiNi**, (2) **3CuCu**, (3) **3CuNi**. Pulse amplitude: 0.025 V.

This trend indicates that some exchange interaction between the two metal centers can exist. In such situations the exchange parameter J can be determined only by means of the magnetization equation.[20,21] The application of the Bleaney−Bowers susceptibility expression would be inappropriate because $J \approx g\beta H$.[22]

$$M = \frac{Ng\,\sinh(g\beta H/kT)}{H[\exp(-2J/kT) + 2\cosh(g\beta H/kT) + 1]} + N_\alpha \quad (1)$$

Here N is Avogadro's number, g is the spectroscopic splitting factor, β is the Bohr magneton, and k is the Boltzmann constant. The Hamiltonian is given by eq 2, where $\hat{\mathbf{S}}$ is the total spin operator ($\hat{S} = \hat{S}_A + \hat{S}_B$) and J expresses the intramolecular exchange interaction between spins:

$$\hat{H}_{ex} = -2J(\hat{S}_A \cdot \hat{S}_B) + g\beta H\hat{S} \quad (2)$$

The best fit parameters $g = 2.06$ and $J = -0.23$ cm^{-1} for 3CuCu, $g = 2.07$ and $J = -0.30$ cm^{-1} for **5CuCu**, and $g = 1.96$ and $J = -0.58$ cm^{-1} for **7CuCu** were obtained with a good agreement factor $R = 1.16 \times 10^{-4}$ for **3CuCu** and $R = 8.55 \times 10^{-5}$ for **5CuCu**, and $R = 2.33 \times 10^{-4}$ for **7CuCu** [$R = \Sigma(M_{exp} - M_{calc})^2/\Sigma(M_{exp})^2$].

The EPR spectra of the compounds (**3CuCu**, **5CuCu**, **7CuCu**, and **9CuCu**) examined at room temperature and 77 K present only single lines of $H \approx 3500$ G for $\nu \approx 9.771$ GHz. The spectroscopic splitting factor was typical for copper(II) centers, with $g \approx 2.04$ for all compounds.

In principle, the observed weak antiferromagnetic interactions in all complexes could be attributed to intramolecular interactions between two paramagnetic centers, which may be transmitted through bonds or space (see structure). The whole situation is even more complex due to delocalization

Table 3. Comparison of the Redox Properties of Homo- and Heterodinuclear Complexes

compd	$E^{\circ\prime}_{Cu}$ (V)	$E^{\circ\prime}_{Ni}$ (V)	$E^{\circ\prime}_{Ni} - E^{\circ\prime}_{Cu}$[a] (V)
7CuCu	1.052		0.274
7NiNi		1.326	
7NiCu	1.045	1.316	0.271
5CuCu	1.084		0.299
5NiNi		1.383	
5NiCu	1.109	1.390	0.281
3CuCu	1.243		
3NiNi		1.485[b]	0.242[b]
		1.585[b]	0.342[c]
3CuNi	1.262	1.558	0.296

[a] The difference between formal potentials of nickel and copper center for hetero- and homodinuclear complex. [b] Ni signals split into two for the dinickel complex with shortest linkers, **3NiNi**.

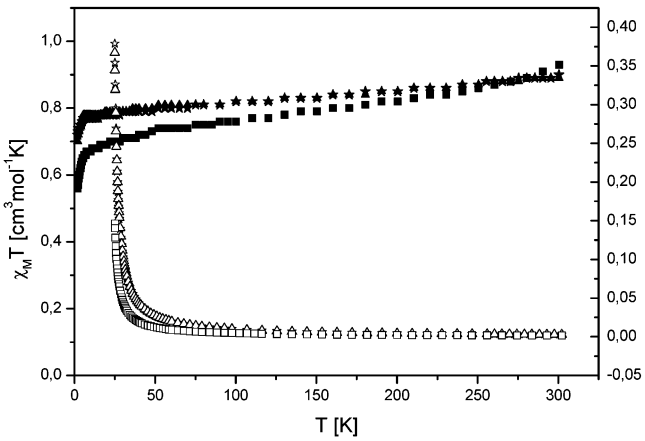

Figure 6. Thermal dependence of χ_M for (☆) **3CuCu,** (△) **5CuCu,** and (□) **7CuCu** and $\chi_M T$ for (★) **3CuCu**, (▲) **5CuCu**, and (■) **7CuCu**. The value of the field is 0.5 T.

(20) Myers, B. E.; Berger, L.; Friendberg, S. A. *J. Appl. Phys.* **1969**, *40*, 1149−1151.
(21) Chiari, B.; Helms, J. H.; Piovesana, O.; Tarantelli, T.; Zanazzi, P. F. *Inorg. Chem.* **1986**, *25*, 2408−2413.
(22) Baran, P.; Koman, M.; Valigura, D.; Mrozinski, J. *J. Chem. Soc., Dalton Trans.* **1991**, 1385−1390.

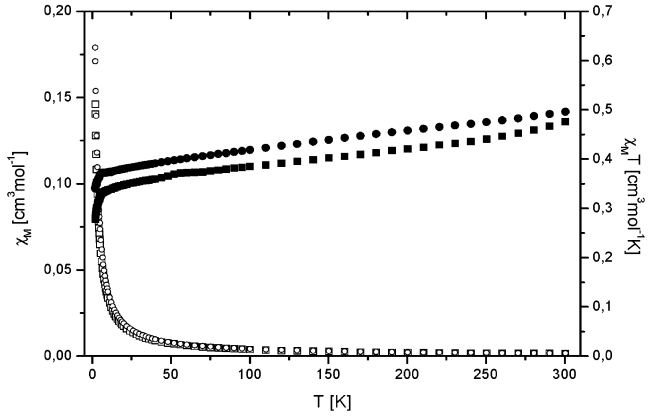

Figure 7. Thermal dependence of χ_M for (□) **7CuCu** and (○) **9CuCu** and $\chi_M T$ for (■) **7CuCu** and (●) **9CuCu**. The value of the field is 0.5 T.

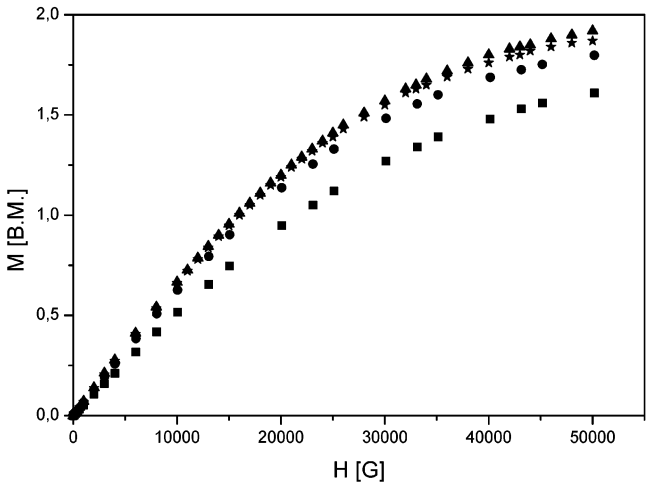

Figure 8. Field dependence of the magnetization at 1.9 K for the following complexes: (★) **3CuCu**; (▲) **5CuCu**; (■) **7CuCu**; (●) **9CuCu**.

of the unpaired electrons over a bigger molecular fragment around the copper centers.

Because magnetic interactions seem to increase with the cavity size, it is quite likely that macrocyclic fragments can interact in an intermolecular manner via hydrogen bonds or/and interactions with counterions. When the ether phenyl rings are located between the macrocyclic fragments (**9CuCu**), a possible charge transfer in such EDA (electron−donor−acceptor) complex can support additional electrostatic interactions.

The magnetic data show that in the **7CuCu** complex there is a slightly stronger exchange interaction between the copper(II) ions than in the catenane **9CuCu** (Figure 7) molecule. This is confirmed by the value of the exchange parameter $J = -0.29$ cm^{-1} for **9CuCu.** The field dependence of magnetization for all complexes at 1.9 K (see Figure 8) clearly supports the occurrence of very weak antiferromagnetic interactions in both complexes. While the magnetization plots for **9CuCu, 5CuCu**, and **3CuCu** tend to a saturation value of about $M = 1.80\ \mu$B/copper(II)−copper(II) pair, the corresponding plots for **7CuCu** presents a maximal value of M equal to 1,61 μB at 5 T.

In consequence, one can say that the interaction between copper(II) centers is higher in the bismacrocycles than in the catenane, which is a trend opposite to that observed in electrochemistry. In our opinion the magnetic interaction decrease on insertion of the benzocrown ether between the macrocyclic units is associated with the shielding role of the former.

On the basis of the molecular structures and the magnetic calculations, all compounds examined behave as weakly interacting dimeric magnets. In the case of the catenane the decrease of $\chi_M T$ values and nonlinear $\chi_M{}^{-1}$ vs T relation at low temperatures are most likely due to an intradimer antiferromagnetic coupling between the copper(II) magnetic centers.

Conclusions

We have synthesized novel heterodinuclear bismacrocyclic complexes of Ni^{II} and Cu^{II} and compared their properties with those of the respective homodinuclear and mononuclear systems. By subtle changes of the structures of the bismacrocyclic units, we modify the strength of interactions between the metallic centers. Homo- and heterodinuclear derivatives (controlled by changing the spacer between the subunits) or catenanes obtained by a preorganization process with π-electron-rich aromatic systems lead to materials with new electrical and magnetic properties. On the basis of molecular structures of all compounds and the results of magnetic measurements we found that examined dicopper compounds behave as weakly interacting dimeric magnets. The electrostatic interactions in the binuclear complexes become stronger with shortening of the alkyl linker. They decrease in the order Ni ···Ni, Ni···Cu, and Cu···Cu, which seems to be related to the number and distribution of the metal center d-electrons. The separations between formal potentials in the complexes may be explained assuming two contributions: electrostatic repulsion between the redox centers or/and electronic coupling between them. Stronger coupling is usually observed for unsaturated bridging units between the redox centers.[23] Very strong electronic coupling between distant metal centers and very high values of comproportionation constants were also found for bis(carbyne) bridging systems.[23,24] In contrast to these compounds, in the complexes studied in this work the contribution of the electrostatic interactions to the observed intramolecular interactions should be favored since no direct metal orbital overlap is possible and the electronic coupling across saturated hydrocarbon spacers is known to be much weaker than in the case of unsaturated bridges.[23−26]

Greater electron density around Cu^{II} cation (d^9) would be expected to show smaller effective electrostatic interactions with the metal cation coordinated in the second macrocyclic ring compared to the respective Ni^{II} complex. Indeed, the intermetallic distance in the bismacrocyclic complexes

(23) Hapiot, P.; Kispert, L. D.; Konovalov, V. V.; Savéant, J.-M. *J. Am. Chem. Soc.* ***2001***, *123*, 6669−6677.
(24) Frohnapfel, D. S.; Woodworth, B. E.; Thorp, H. H.; Templeton, J. L. *J. Phys. Chem. A* **1998**, *102*, 5665−5669.
(25) Brady, M.; Weng, W.; Zhou, Y.; Seyler, J. W.; Amoroso, A.; Arif, A. A.; Böhme, M.; Frenking, G.; Gladysz, J. A. *J. Am. Chem. Soc.* **1997**, *119*, 775−788.
(26) LeNarvor, N.; Toupet, L.; Lapinte, C. J. *Am. Chem. Soc.* ***1995***, *117*, 7129−7138.

decreases with the increasing number of d electrons: **3NiNi** (d^8d^8), **3CuNi** (d^9d^8), **3CuCu** (d^9d^9).

Introduction of an electron-donating guest between the bismacrocyclic fragments increases the separation of formal potentials of the centers revealing interactions of one of them with the electron-rich ring. In this case, the potentials should be affected not only by electrostatic effects between the redox centers but also by the nonequivalency of the centers due to the different microenvironments around them. Similar microenvironmental effects were demonstrated using several techniques for other types of catenanes and rotaxanes.[27]

(27) Anelli P. L.; Ashton, P. R.; Ballardini, R.; Balzani, V.; Delgado, M.; Gandolfi, M. T.; Goodnow, T. T.; Kaifer, A. E.; Philp, D.; Pietraszkiewicz, M.; Prodi, L.; Reddington, A. M. Z.; Spencer, N.; Stoddart, J. F.; Vicent, C.; Williams, D. J. *J. Am. Chem. Soc.* **1992**, *114*, 193−218.

The synthetic strategy proposed in this work may be applied to obtain catenanes with heterodinuclear transition metal complexes of bismacrocycles. Work in this direction is continuing in our laboratories.

Acknowledgment. Financial support by the State Committee for Scientific Research (Projects 3 T09A 076 15, 4 T09A 048 23, and 4 T09A 109 22) is gratefully acknowledged. The X-ray measurements were undertaken in the Crystallographic Unit of the Physical Chemistry Laboratory at the Chemistry Department of the University of Warsaw.

Supporting Information Available: Tables of hydrogen bond parameters for bismacrocycles studied. This material is available free of charge via the Internet at http://pubs.acs.org.

IC034127B